pattern, whereas its Mn(II) complex was obtained in a crystalline form. The framework of the 24-membered ring is probably too flexible to maintain a well-defined ring conformation. Chelate formation with metal ions makes the ring rigid and results in a well-defined configuration of the chelate ring. The structural integrity of the metal chelate rings leads to the formation of crystals of the metal chelate. Extensive hydrogen bonding occurs in the crystal lattice and defines the arrangement of the metal chelate molecules in the crystal. A water molecule (denoted OW2 in Figure 2) occupies a special position on the crystal C_2 axis that coincides with the C_2 axis of a metal chelate ring. This water molecule forms strong hydrogen bonds with two water molecules (denoted OW1 in Figure 2) coordinated to Mn and also with two amide oxygen atoms (O6) that are weakly bonded to Mn. These hydrogen bonds firmly link the two Mn ions within a chelate ring and define the molecular structure of the metal chelate.

In conclusion, the X-ray crystal analyses of the metal complexes have confirmed the formation of the new 12-membered and the 24-membered macrocycles. The new macrocyclic ligands are expected to form stable chelates with a variety of metal ions. One of the features of the synthetic method for the ligands is that the macrocyclic ring can be prepared in one step in a high yield without using template metal ions. The same method is expected to be useful for the synthesis of a series of macrocycles having different ring sizes and different numbers of pendent acetato groups.

Acknowledgment. The work at the Universidad de Sonora was supported by the Consejo Nacional de Ciencia y Tecnología, Mexico (Grant No. 0204-E9107-2207).

Supplementary Material Available: Tables of crystallographic experimental details, thermal parameters, positional parameters of hydrogen, and additional bond lengths and angles and ORTEP diagrams of the unit cells for $CuL(12)\cdot 4H_2O$ and $Mn_2L(24)\cdot 8H_2O$ and a table of least-squares planes for $CuL(12)\cdot 4H_2O$ (14 pages); listings of observed and calculated structure factors for the two compounds (23 pages). Ordering information is given on any current masthead page.

Contribution from the Chemistry Department, Washington State University, Pullman, Washington 99164-4630, and Argonne National Laboratory, Argonne, Illinois 60439

Synthesis and Characterization of the Pseudo-1-D Mixed-Valence $(Et_{4-n}Me_nN)Cu_2X_4$ Salts: Pinned Charge Density Wave Systems Exhibiting Intervalence Charge Transfer

Brian Scott,[†,‡] Roger Willett,*[,‡] Leigh Porter,[§] and Jack Williams[§]

Received April 3, 1991

A series of mixed-valence Cu(I)/Cu(II) linear chain compounds exhibiting pinned charge density waves have been synthesized. The compounds have stoichiometry $ACu^{I}Cu^{II}X_4$ with X = Cl or Br and A = tetraethylammonium (TEA), triethylmethylammonium (TEM), or diethyldimethylammonium (DEM). The crystal structures of the bromide analogues have been determined. The $(TEM)Cu_2Br_4$ salt is tetragonal, with space group $P4_2/ncm$, a = 10.812 (1) Å, c = 13.234 (2) Å, V = 1546.9 (4) Å^3, Z = 4, d_x = 2.42 g/cm^3, and R = 0.0647. The $(DEM)Cu_2Br_4$ salt is also tetragonal, with space group $P4_2/ncm$, a = 10.523 (1) Å, c = 13.1630 (9) Å, V = 1457.5 (4) Å^3, Z = 4, d_x = 2.50 g/cm^3, and R = 0.0974. The $(TEA)Cu_2Br_4$ salt is orthorhombic, with space group $P2_12_12_1$, a = 11.084 (2) Å, b = 19.696 (3) Å, c = 21.847 (2) Å, V = 4770 (1) Å^3, Z = 12, d_x = 2.41 g/cm^3, and R = 0.0358. These structures reveal infinite chains of alternating $Cu^{I}X_4^{3-}$ and $Cu^{II}X_4^{2-}$ tetrahedra (distorted) sharing edges, the chains being effectively isolated by bulky tetraalkylammonium cations. Although the valence states appear to be localized, with a 0.1 Å difference in the Cu(I)–X and Cu(II)–X bond lengths, several characterization techniques indicate Robin and Day class II behavior. The data also support a Peierls $4k_f$ distorted charge density wave state for these chains. All salts show an intervalence charge-transfer band in the visible region of the spectrum. Conductivity measurements indicate semiconductive behavior. Temperature-dependent magnetic susceptibility measurements on $(TEA)Cu_2Br_4$ reveal weak antiferromagnetic coupling, which is attributed to short Br···Br contacts between $Cu^{II}X_4^{2-}$ species within the chains. The above physical properties are rationalized in light of previous EHMO band calculations.

Introduction

A recent endeavor in this laboratory has focused on the design, synthesis, and characterization of low-dimensional, mixed-valence copper halide systems.[1] The main goal behind this research is to discover new systems which exhibit intervalence charge transfer and conductivity. The advent of the copper oxide superconductors, which show copper in different oxidation states and low-dimensional networks, have given this work added significance.[2] There has also been speculation that the trigonal-planar copper species present in the record T_c organic superconductors is of mixed-valence character; it is true that the superconduction is taking place in the organic stacks in these systems, but the role of the co-crystallite copper species is not fully understood.[3] The structural instabilities that low-dimensional materials often exhibit is another factor which adds interest to these compounds.[4]

The mixed-valence chemistry of copper(II)–copper(I) halide compounds is very rich. These compounds fall into two classes; one class containing isolated copper(I) and copper(II) species, the other containing bridging halide ions between the copper(II) and copper(I) centers. The latter class of compounds may, or may not, exhibit intervalence charge transfer, depending on the nature of the Cu(II)–X–Cu(I) bridge. These classes correspond to the Robin and Day classes I and II.[5] The former class contains compounds such as $(Bu_4N)_3Cu_3Cl_8(L)$ (where L = CH_3NO_2, CH_3CN, etc.), which is currently being characterized in this laboratory. This mixed-valence salt contains isolated $Cu_2Cl_6^{2-}$ and $CuCl_2L^-$ anions, and thus no pathway for intervalence charge transfer.[6] The latter class contains a myriad of interesting compounds. The classic example of this is the $Co(NH_3)_6Cu$-

[†] Present location: Inorganic and Structural Chemistry Group (INC-4), Isotope and Nuclear Chemistry Division, Los Alamos National Laboratory, Los Alamos, NM 87544.
[‡] Washington State University.
[§] Argonne National Laboratory.

(1) (a) Willett, R. D. *Inorg. Chem.* **1987**, *26*, 3424. (b) Willett, R. D.; Halvorson, K. *Acta Crystallogr.* **1988**, *C44*, 2068. (c) Scott, B.; Willett, R. D. *Inorg. Chem.* **1991**, *30*, 110. (d) Scott, B.; Willett, R. D. *Acta Crystallogr.* **1991**, *C47*, 1389.
(2) Sleight, A. W. *Science* **1988**, *242*, 1519.
(3) Kewamoto, A.; Tanaka, J.; Tanaka, M. *Acta Crystallogr.* **1987**, *C43*, 205.
(4) Hoffmann, R. *Solids and Surfaces: A Chemist's View of Bonding in Extended Structures*; VCH: New York, 1988.
(5) Robin, M. B.; Day, P. *Adv. Inorg. Chem. Radiochem.* **1967**, *10*, 248.
(6) Willett, R. D. Personal communication.

0020-1669/92/1331-2483$03.00/0

Cl_5–$[Co(NH_3)_6]_4Cu_5Cl_{17}$ system, in which the former contains square-pyramidal $CuCl_5^{3-}$ anions while the latter contains a cluster of four $CuCl_4^{3-}$ anions linked tetrahedrally to a central Cu(I) ion.[7] In the mixed-valence regime, a new, rather weak, band was found in the middle of the visible region of the spectrum. Also in this category, and recently characterized in this laboratory, is the $(hydrazinium)_2Cu_3Cl_6$ system.[1c] This salt contains square-planar, four-coordinate $Cu(N_2H_5)_2Cl_2$ species in which the axial (as well as the equatorial) chlorine sites are occupied by bridges to trigonal-planar $CuCl_3^{2-}$ anions. A broad intervalence transition, at approximately 18 000 cm^{-1}, has been identified in this compound. There also exists a group of halide-bridged, Cu(I)/Cu(II) compounds which have not been assigned to either class I or class II due to a lack of experimental data at this time. The compound $[(3\text{-aminopyridinium})_4Cu_4Br_{10}]$, the subject of a crystallographic study in this laboratory, falls into this category, showing square-pyramidal copper(II) sites and tetrahedral copper(I) sites bridged by chlorine atoms.[1b] The salt $Cu^{II}Cu^{I}(4\text{-metz})_4Cl_3$, where 4-metz represents 4-methylthiazole, possesses a $Cu^{I}Cu^{II}Cl_2$ bridging unit, with the copper(II) center in a distorted tetragonal-pyramidal site, the copper(I) center in a distorted tetrahedral site.[8] Another salt recently studied by the authors is $(benzylviologen)Cu_3Cl_9(H_2O)$. This compound consists of trimers of loosely associated $CuCl_4^{2-}$, $CuCl_2^-$, and $CuCl_3(H_2O)^-$ anions.[1d] These trimers are hydrogen-bonded into chains, and the anions within the trimers are held together via Cu(I)···Cl–Cu(II) linkages. However, the length of the Cu(I)···Cl linkages probably indicate only weak intervalence interactions. A whole class of $[Cu^{II}A_n][Cu^{I}X_2]_2$ compounds, where $n = 2$ for bidentate and $n = 4$ for monodentate ligands, exists.[9] The majority of these materials contain infinite chains of CuX_4^{3-} tetrahedra sharing edges. The bridging halides in these chains occupy axial positions of the $Cu^{II}A_n$ species, the two axial sites being occupied by bridging halides from adjacent chains. This bridging network is made up of Cu(II)···X–Cu(I) linkages. In these compounds, the length of the Cu(II)···X linkages probably indicate only weak intervalence interactions.

The title compounds also fit into the class of halogen-bridged, mixed-valence metal materials. These compounds include Wolfframs Red salt and its derivatives,[10] a group of compounds containing chains composed of stacked, alternating, square-planar $Pt^{II}L_4$ and octahedral $Pt^{IV}L_4X_2$ units. These systems are Peierls-distorted solids in which a dimerization of the bridging halide ions leads to a trapped charge density wave. It will be shown that they have much in common with the title compounds. However, at the same time, the title compounds possess their own unique properties that make them good systems for elucidating the properties of charge density wave materials.

The focus of this paper will be on a series of mixed-valence Cu(I)/Cu(II) halide chains of stoichiometry ACu_2X_4. The initial report on the structure of $(TEA)Cu_2Cl_4$ demonstrated the existence of chains of edge-shared $CuCl_4$ tetrahedra with alternating, localized Cu(I) and Cu(II) sites.[1a] The ubiquitous D_{2d}-type compression of the Cu(II) coordination sphere is exhibited as a distortion of the chain structure. In the idealized undistorted structure, the dihedral angle between the two bridging CuX_2 planes at each site would be 90°. However, in the actual structure, these planes are twisted so that the observed dihedral angle is 90° ± θ at alternating Cu(II) sites, with $\theta = 27.3°$. Subsequent to the report of the $(TEA)Cu_2Cl_4$ structure, Sherwood and Hoffmann[11] examined the band structure of the chains. They demonstrated that the chain structure corresponded to a Peierls-distorted system which leads to a strongly trapped charge density wave. However, in contrast to the mixed-valence Pt(II)/Pt(IV) halide chains, the driving force for the dimerization (and subsequent charge localization) of the chain is the twist distortion described above.

The main question to be answered in this work is the extent of the electron delocalization within the copper halide chains. Absorption spectroscopy, X-ray crystallography, and magnetic susceptibility results will be used to answer this question. Another important point which will be investigated is the nature of the chain structure; the question of whether, or not, the structure is dominated by electronic effects (i.e. distortions brought on by partially filled bands) or by crystal packing forces will be dealt with. It will be argued that the above experimental data support the Sherwood and Hoffmann picture.

Table I. Crystallographic Data for $(TEA)Cu_2Br_4$, $(TEM)Cu_2Br_4$, and $(DEM)Cu_2Br_4$

compd	$TEACu_2Br_4$	$TEMCu_2Br_4$	$DEMCu_2Br_4$
chem formula	$C_8H_{20}Br_4Cu_2N$	$C_7H_{18}Br_4Cu_2N$	$C_6H_{16}Br_4Cu_2N$
fw	576.96	562.93	550.92
a, Å	11.084 (2)	10.812 (1)	10.523 (1)
b, Å	19.696 (3)		
c, Å	21.847 (2)	13.234 (2)	13.1630 (9)
V, Å^3	4770 (1)	1546.9 (4)	1457.5 (4)
Z	12	4	4
space group	$P2_12_12_1$ (No. 19)	$P4_2/ncm$ (No. 138)	$P4_2/ncm$ (No. 138)
T, °C	−150	22	22
λ, Å	1.541 78	1.541 78	0.710 69
ρ_{calcd}, g cm^{-3}	2.41	2.42	2.50
μ, cm^{-1}	150.1	154.0	137.2
transm coeff	0.020–0.13	0.65–0.96	0.14–0.95
$R(F_o)$	0.0358	0.0647	0.0974
$R_w(F_o)$	0.0397	0.0869	0.0948

Experimental Section

Synthesis. All title compounds were prepared by dissolving, with heat, stoichiometric amounts of CuX, CuX_2, and the appropriate cation in a 1:3 ethanol:concentrated HX solution. The solution was allowed to evaporate slowly at room temperature under a nitrogen atmosphere. This eventually produced long, thin needles (deep blue for the chloride and deep green for the bromide) for all analogues except for $(TEA)Cu_2Br_4$, which formed thin green plates. $(TEA)Cu_2Br_4$ crystals grown out of a 1:3 concentrated HBr:ethyl acetate solution formed well-shaped octahedra. Freshly prepared CuX is the most critical aspect of this synthesis and should be pure white for the best results (the CuX compounds were purified using ascorbic acid). An inert atmosphere is essential for the chloride analogues, in order to prevent air oxidation of the copper(I) species. All of the chloride analogues, except for the TEA salt, form impure and unstable crystals, none of which were suitable for any characterization studies.

X-ray Structure. Structure determinations for $(TEM)Cu_2Br_4$, $(TEA)Cu_2Br_4$, and $(DEM)Cu_2Br_4$ were carried out. The structure of $(TEA)Cu_2Cl_4$ has been reported previously.[1a]

An approximately octahedral-shaped crystal of $(TEA)Cu_2Br_4$, with well-defined faces, was selected for data collection. The basal plane of the crystal had dimensions 0.43 × 0.47 mm^2, with an equatorial length equal to 0.22 mm. The eight faces of the crystal belonged to [011] and [102]. The data were collected at −150 °C due to excessive thermal motion at room temperature. The data were collected on a Nicolet R3 diffractometer with graphite-monochromatized Cu Kα (λ = 1.541 78 Å) radiation.[12] A Nicolet LT-2 low-temperature device was used to cool the crystal. The lattice constants were optimized from the least-squares refinement to the angular settings of 25 carefully centered reflections in the range $77° < 2\theta < 84°$. Two standard reflections (1,0,14, 467) were monitored every 96 reflections and showed no systematic variation. The intensities of 3388 reflections were measured using an ω scan (0.9° range) with speeds varying from 4 to 29.3°/min. Following the data reduction, 3360 unique reflections remained, with 3280 having $|F| > 3\sigma(F)$. All non-hydrogen atoms were refined anisotropically to a final $R = 0.0358$

(7) (a) Culpin, D.; Day, P.; Edwards, P. R.; Williams, R. J. P. *J. Chem. Soc. C* **1968**, 1835, 1838. (b) Mori, M. *J. Chem. Soc. Jpn.* **1960**, *33*, 985. (c) *Ibid.* **1961**, *34*, 454 and 1249. (d) Reinen, D.; Friebel, C. *Inorg. Chem.* **1984**, *23*, 791. (e) Murray-Rust, P. *Acta Crystallogr.* **1973**, *B29*, 2559.

(8) Marsh, W. E.; Hatfield, W. E.; Hodgson, D. J. *Inorg. Chem.* **1983**, *22*, 2899.

(9) (a) Simonsen, O.; Toftlund, H. *Acta Crystallogr.* **1987**, *C43*, 831. (b) Baglio, J. A.; Weakliem, H. A.; Demilio, F.; Vaughan, P. A. *J. Inorg. Nucl. Chem.* **1970**, *32*, 795. (c) Baglio, J. A.; Vaughan, P. A. *J. Inorg. Nucl. Chem.* **1970**, *32*, 803.

(10) Ueta, M.; Kanzaki, H.; Kobayashi, K.; Toyozawa, Y.; Hanamura, E. *Excitonic Processes in Solids*; Springer Series in Solid-State Sciences; Springer; Berlin, 1986; Vol. 60, Chapter 9.

(11) Sherwood, P.; Hoffmann, R. *Inorg. Chem.* **1989**, *28*, 509.

(12) Campana, C. F.; Shepard, D. F.; Litchman, W. M. *Inorg. Chem.* **1981**, *20*, 4039.

and $R_w = 0.0397$. The final refinement included 308 least-squares parameters. The goodness of fit was 1.641, and the final difference map showed a residual of 0.8 e Å^{-3} near Cu(1). The hydrogen atoms were refined isotropically with the C–H distances fixed at 0.96 Å and the isotropic thermal parameters fixed at 1.2 times the equivalent isotropic U of the atom to which they were bonded. Numerical absorption corrections were applied. The SHELXTL 5.1 software package was used for data reduction and refinement.[13] Table I gives a summary of important crystal parameters.

A needle-shaped crystal of $(TEM)Cu_2Br_4$ with dimensions 0.21 × 0.062 × 0.042 mm^3 was mounted on a thin glass fiber, and reflection data were collected using the same experimental setup as for $(TEA)Cu_2Br_4$ (minus the low-temperature apparatus). The lattice constants were optimized as described above for the $(TEA)Cu_2Br_4$ salt using reflections in the range $55 < 2\theta < 72°$. The standard reflections (2,–1,–2, 0,–3,–2) were monitored every 96 reflections and showed no systematic variation. The intensities of 1088 reflections were measured using an ω scan (1.0°) with speeds varying from 4 to 29.3°/min. Following data reduction, 527 reflections remained, with 464 having $|F| > 3\sigma(F)$. The Cu, Br, and N atoms were refined with anisotropic thermal parameters. The C atoms were refined with isotropic thermal parameters. The N atom resides on a site of *mm* (C_{2v}) symmetry, and thus the TEM cation must be disordered. A methyl group was fixed on one of the mirror planes; an extended ethyl group, on the other. A carbon atom was also placed directly above the nitrogen atom on the C_2 symmetry axis; it was postulated that the two extended ethyl groups were sitting on one of the mirror planes and that the other mirror plane contained a methyl group and an ethyl group with its terminal C atom folded up onto the C_2 axis. It is believed that this conformation and its mirror image are evenly distributed among the unit cells of the crystal, thus accounting for the *mm* site symmetry of the TEM cation. The final refinement yielded $R = 0.0647$ and $R_w = 0.0869$ and included 41 least-squares parameters. The goodness of fit was 1.053, and the final difference map showed a residual of 1.25 e Å^{-3} near Br. The hydrogen atoms were refined with isotropic thermal parameters fixed at 1.2 times the equivalent isotropic U of the atom to which they were bonded. C–H distances were fixed at 0.96 Å. Numerical absorption corrections were applied. Table I gives a summary of important crystal parameters.

A needle-shaped crystal of $(DEM)Cu_2Br_4$ with dimensions 0.17 × 0.17 × 0.33 mm^3 was mounted on a glass fiber, and reflection data were collected on a Syntex $P2_1$ diffractometer upgraded to Nicolet R3 specifications.[12] Monochromatized Mo Kα ($\lambda = 0.71069$ Å) radiation was used. The lattice constants were determined as described above using reflections in the range $35 < 2\theta < 40°$. Two standard reflections (032, 004) were monitored every 96 reflections and showed no systematic variation. The intensities of 1141 reflections were measured using an ω scan (1.0°) with speeds varying from 4 to 29.3°/min. Following data reduction, 525 unique reflections remained, with 352 having $|F| > 3\sigma(F)$. Numerical absorption corrections were applied. The Cu, Br, and N atoms were refined with anisotropic thermal parameters. The C atoms were refined with isotropic thermal parameters. The final refinement resulted in $R = 0.0974$ and $R_w = 0.0948$ and included 36 least-squares parameters. The goodness of fit was 1.314, and the final difference map showed a residual of 1.5 e Å^{-3} near N. Attempts to model this residual as disorder in the DEM cation were not successful, and the high R value is attributed to this inability to accurately model the counterion. (The N atom resides on a *mm* site of symmetry and thus is intersected by two perpendicular mirror planes. A methyl group was placed on one of these mirror planes, with an ethyl group on the other. It is postulated that the terminal carbons of the ethyl groups were disordered over two positions, but the residual electron density could not be modeled in this fashion.) The hydrogen atoms were treated as in the TEM salt. Table I gives a summary of important crystal parameters.

Absorption Spectroscopy. The single-crystal, polarized absorption spectrum for the $(TEA)Cu_2Br_4$ analogue, in the range 850–500 nm, was taken on a Perkin-Elmer 330 spectrophotometer fitted with condensing optics. A thin, crystalline plate was mounted over a pinhole in an aluminum foil mask. The source was polarized using a sheet of polaroid film, and the crystal was mounted so that the light path was traveling parallel to (100). Two polarized spectra were taken: one with the electric vector lying parallel to the $[Cu^{II}Cu^{I}Br_4]_\infty$ chain axis and one perpendicular to this chain axis. Crystalline flakes of the $(TEA)Cu_2Cl_4$ analogue, suitable for single-crystal polarized spectra on the Perkin-Elmer 1700X FTIR instrument, were obtained by shattering large crystals. The source was polarized both perpendicular and parallel to the $[Cu^{I}Cu^{II}Cl_4]_\infty$ chain axis using a sheet of polaroid film. The single-crystal spectra of $(TEM)Cu_2Br_4$ and $(DEM)Cu_2Br_4$ could not be measured in this fashion due to the intense absorption these compounds display in this region. The crystals were observed under a microscope before and after the absorption experiments. No decomposition was noted.

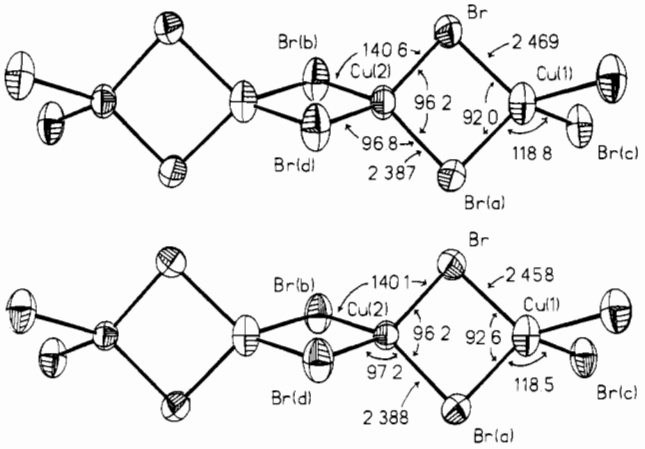

Figure 1. (a, Top) portion of the $[Cu_2Br_4]_\infty$ chain in $(TEM)Cu_2Br_4$ showing thermal ellipsoids. The Cu(I) and Cu(II) sites are labeled Cu(1) and Cu(2), respectively. (b, Bottom) portion of the $[Cu_2Br_4]_\infty$ chain in $(DEM)Cu_2Br_4$ showing thermal ellipsoids. The Cu(I) and Cu(II) sites are labeled Cu(1) and Cu(2), respectively.

Thin film spectra of $(TEA)Cu_2Cl_4$, $(DEM)Cu_2Br_4$, and $(TEM)Cu_2Br_4$ were taken of samples created by melting the crystals between two glass slides. They were taken on the Perkin-Elmer 330 system in the range 850–500 nm. The spectra of $(TEA)Cu_2Br_4$, $(DEM)Cu_2Br_4$, and $(TEM)Cu_2Br_4$ were taken in the range 3000–12000 cm^{-1} on a Perkin-Elmer 1700X FTIR instrument at both room temperature and 77 K. The spectra for the $(TEA)Cu_2Cl_4$, $(DEM)Cu_2Br_4$, and $(TEM)Cu_2Br_4$ analogues were taken in this fashion since their tetragonal nature precluded plate growth, which is a necessary condition for measuring the single-crystal spectra of these intensely absorbing compounds on a Perkin-Elmer 330 system. The spectrum of $(TEA)Cu_2Br_4$ was taken in this fashion because even very thin crystals were opaque in the NIR region. The color of the melt was examined closely under a microscope to ensure no decomposition had occurred. The $(TEM)Cu_2Cl_4$ and $(DEM)Cu_2Cl_4$ analogues decomposed during the melting process, and thus the spectra for these two compounds could not be measured.

Electrical Conductivities. The room-temperature conductivities, carried out on $(TEA)Cu_2Br_4$ and $(TEA)Cu_2Cl_4$, were measured at Argonne National Laboratory. The standard four-probe, dc measurement technique was used.[14] Due to the presence of halide ions two measurements on each compound were made, using both gold and silver pastes to attach the gold leads to the crystals. These two methods showed no difference in the measured resistivities. The resistivities were measured along the chain/needle axis.

Magnetic Susceptibilities. The temperature-dependent, powder susceptibilities of the $(TEA)Cu_2Br_4$ analogue was measured at Montana State University on a Princeton Applied Research 151 vibrating sample magnetometer. Measurements were made in the temperature range 4–100 K. The field was a constant 5000 G throughout the data collection, and a separate field vs magnetization data collection for 0–5000 G showed no saturation.

EHMO Band Calculations. These calculations were carried out previously by Sherwood and Hoffmann on the $(TEA)Cu_2Cl_4$ salt in order to gain more insight into the physical properties of this compound.[11] The predictions resulting from these calculations were primarily concerned with the structural distortions of such low-dimensional chains, as well as their magnetic and electronic properties. These predictions will be discussed in light of new data presented in this paper. In addition, these results will be used to help understand the origin of the absorption spectra of the title compounds. All of the details surrounding these calculations may be found in the previous work.

Results and Analysis

X-ray Structures. The $(TEM)Cu_2Br_4$ and $(DEM)Cu_2Br_4$ structures contain infinite chains of $Cu^{II}Br_4^{2-}$ and $Cu^{I}Br_4^{3-}$ anions sharing edges (Figure 1). These two structures are tetragonal with space group $P4_2/ncm$. The symmetry of these two structures is commensurate with the high symmetry of the sites occupied

(13) Sheldrick, G. *SHELXTL Users Manual*, Version 5.1; Nicolet Analytical Instruments: Madison, WI, 1986.

(14) Cheetham, A. K.; Day, P. *Solid State Chemistry Techniques*; Clarendon Press, Oxford, U.K., 1987.

Table II. Atomic Coordinates ($\times 10^4$) and Isotropic Thermal Parameters ($Å^2 \times 10^3$) for $(TEM)Cu_2Br_4$, $(DEM)Cu_2Br_4$, and $(TEA)Cu_2Br_4$

atom	x	y	z	U^a
		TEM		
Cu(1)	7500	2500	2500	78 (1)*
Cu(2)	7500	2500	10000	55 (1)*
Br	6990 (2)	938 (1)	6204 (1)	75 (1)*
N	2500	2500	6134 (13)	74 (6)*
C12	4176 (20)	4176 (20)	6215 (17)	108 (8)
C12′	2500	2500	4696 (50)	126 (22)
C1	3366 (67)	3366 (67)	6018 (50)	581 (88)
C2	3658 (50)	1342 (50)	7046 (40)	326 (32)
		DEM		
Cu(1)	7500	2500	2500	79 (4)*
Cu(2)	7500	2500	10000	45 (2)*
Br	6986 (4)	893 (3)	6211 (2)	69 (2)*
N	2500	2500	6359 (24)	31 (8)*
C12	4251 (59)	4251 (59)	6297 (38)	139 (25)
C1	3336 (35)	3336 (35)	5753 (61)	388 (84)
C2	3449 (28)	1551 (28)	6692 (91)	431 (97)
		TEA		
Cu(1)	8006 (2)	782 (1)	1265 (1)	28 (1)*
Cu(2)	7976 (1)	2457 (1)	1336 (1)	20 (1)*
Cu(3)	7943 (2)	4149 (1)	1299 (1)	31 (1)*
Cu(4)	7955 (1)	5797 (1)	1175 (1)	21 (1)*
Cu(5)	7896 (2)	7446 (1)	1125 (1)	32 (1)*
Cu(6)	7910 (2)	9123 (1)	1188 (1)	22 (1)*
Br(1)	6335 (1)	−42 (1)	1220 (1)	28 (1)*
Br(2)	9562 (1)	−96 (1)	1238 (1)	26 (1)*
Br(3)	7558 (1)	1603 (1)	2083 (1)	28 (1)*
Br(4)	8390 (1)	1688 (1)	514 (1)	25 (1)*
Br(5)	6424 (1)	3264 (1)	1570 (1)	25 (1)*
Br(6)	9523 (1)	3281 (1)	1163 (1)	27 (1)*
Br(7)	8108 (1)	5069 (1)	2053 (1)	26 (1)*
Br(8)	7812 (1)	4923 (1)	414 (1)	29 (1)*
Br(9)	6434 (1)	6565 (1)	827 (1)	26 (1)*
Br(10)	9475 (1)	6617 (1)	1413 (1)	27 (1)*
Br(11)	7080 (1)	8284 (1)	1869 (1)	28 (1)*
Br(12)	8644 (1)	8347 (1)	442 (1)	30 (1)*
N(1)	2962 (7)	8289 (4)	1265 (3)	22 (2)*
N(2)	2932 (8)	1743 (4)	1274 (3)	22 (2)*
N(3)	2973 (8)	4808 (4)	1313 (4)	26 (2)*
C(11)	3475 (11)	8897 (5)	1621 (5)	35 (3)*
C(12)	3057 (11)	9588 (5)	1396 (5)	35 (3)*
C(13)	1621 (10)	8289 (5)	1329 (4)	30 (2)*
C(14)	1109 (10)	8270 (5)	1981 (5)	28 (2)*
C(15)	3282 (10)	8322 (5)	596 (5)	33 (2)*
C(16)	4624 (10)	8319 (5)	449 (5)	33 (3)*
C(17)	3535 (11)	7680 (5)	1567 (5)	33 (3)*
C(18)	3096 (11)	6987 (6)	1289 (5)	39 (3)*
C(21)	3863 (10)	1294 (5)	946 (5)	27 (2)*
C(22)	4871 (10)	1671 (5)	623 (5)	34 (2)*
C(23)	2371 (11)	2229 (5)	834 (5)	30 (2)*
C(24)	1784 (12)	1886 (5)	258 (5)	41 (3)*
C(25)	2034 (10)	1268 (5)	1548 (5)	29 (2)*
C(26)	986 (10)	1611 (5)	1875 (5)	31 (2)*
C(27)	3518 (12)	2179 (5)	1766 (5)	38 (3)*
C(28)	4073 (11)	1764 (6)	2292 (5)	40 (3)*
C(31)	3785 (11)	5224 (5)	1730 (5)	36 (3)*
C(32)	4635 (13)	4813 (6)	2125 (6)	52 (3)*
C(33)	3708 (12)	4377 (5)	877 (5)	39 (3)*
C(34)	4523 (13)	4766 (6)	444 (6)	53 (4)*
C(35)	2209 (11)	5300 (5)	964 (5)	35 (3)*
C(36)	1306 (13)	4983 (7)	548 (7)	61 (4)*
C(37)	2222 (11)	4314 (5)	1699 (5)	36 (3)*
C(38)	1423 (14)	4687 (7)	2167 (7)	62 (4)*

[a] All entries with an asterisk refer to atoms refined with the equivalent isotropic U defined as one-third of the trace of the orthogonalized U_{ij} tensor.

by the copper(II) and copper(I) ions. The copper(II) ions sit on sites of D_2 symmetry, with the actual $Cu^{II}Br_4$ geometry very close to D_{2d}. The copper(I) ions sit on sites of S_4 symmetry. There are two copper(II) ions and two copper(I) ions in the repeat unit, with a Cu(II)–Cu(I) distance of 3.308 Å for the TEM salt and 3.294 Å for the DEM salt. The overall chain structure is best

Table III. Bond Distances (Å) and Angles (deg) for the $Cu_2Br_4^-$ Portion of $TEMCu_2Br_4$, $DEMCu_2Br_4$, and $TEACu_2Br_4$

		TEM[a]	
Cu(1)–Br	2.469 (1)	Cu(2)–Br	2.387 (1)
Br–Cu(1)–Br(a)	92.0 (1)	Br–Cu(2)–Br(b)	140.6 (1)
Br–Cu(2)–Br(a)	96.2 (1)	Br(a)–Cu(2)–Br(d)	96.8 (1)
Br(a)–Cu(1)–Br(c)	118.8 (1)		
		DEM[a]	
Cu(1)–Br	2.458 (3)	Cu(2)–Br	2.388 (3)
Br–Cu(1)–Br(a)	92.6 (1)	Br–Cu(2)–Br(b)	140.1 (2)
Br–Cu(2)–Br(a)	96.2 (1)	Br(a)–Cu(2)–Br(d)	97.2 (2)
Br(a)–Cu(1)–Br(c)	118.5 (1)		
		TEA[b]	
Cu(1)–Br(1)	2.464 (2)	Cu(4)–Br(7)	2.400 (2)
Cu(1)–Br(2)	2.443 (2)	Cu(4)–Br(8)	2.399 (2)
Cu(1)–Br(3)	2.462 (2)	Cu(4)–Br(9)	2.390 (2)
Cu(1)–Br(4)	2.461 (2)	Cu(4)–Br(10)	2.392 (2)
Cu(2)–Br(3)	2.389 (2)	Cu(5)–Br(9)	2.462 (2)
Cu(2)–Br(4)	2.393 (2)	Cu(5)–Br(10)	2.475 (2)
Cu(2)–Br(5)	2.399 (2)	Cu(5)–Br(11)	2.487 (2)
Cu(2)–Br(6)	2.391 (2)	Cu(5)–Br(12)	2.463 (2)
Cu(3)–Br(5)	2.494 (2)	Cu(6)–Br(11)	2.406 (2)
Cu(3)–Br(6)	2.466 (2)	Cu(6)–Br(12)	2.379 (2)
Cu(3)–Br(7)	2.456 (2)	Cu(6)–Br(1a)	2.399 (2)
Cu(3)–Br(8)	2.468 (2)	Cu(6)–Br(2a)	2.394 (2)
Br(1)–Cu(1)–Br(2)	93.6 (1)	Br(9)–Cu(5)–Br(11)	113.7 (1)
Br(1)–Cu(1)–Br(3)	108.1 (1)	Br(10)–Cu(5)–Br(11)	121.9 (1)
Br(2)–Cu(1)–Br(3)	128.6 (1)	Br(9)–Cu(5)–Br(12)	124.7 (1)
Br(1)–Cu(1)–Br(4)	125.5 (1)	Br(10)–Cu(5)–Br(12)	113.0 (1)
Br(2)–Cu(1)–Br(4)	112.0 (1)	Br(11)–Cu(5)–Br(12)	92.3 (1)
Br(3)–Cu(1)–Br(4)	92.5 (1)	Br(11)–Cu(6)–Br(12)	96.5 (1)
Br(3)–Cu(2)–Br(4)	96.0 (1)	Br(11)–Cu(6)–Br(1a)	100.1 (1)
Br(3)–Cu(2)–Br(5)	100.4 (1)	Br(12)–Cu(6)–Br(1a)	135.2 (1)
Br(4)–Cu(2)–Br(5)	135.8 (1)	Br(11)–Cu(6)–Br(2a)	134.9 (1)
Br(3)–Cu(2)–Br(6)	136.5 (1)	Br(12)–Cu(6)–Br(2a)	100.5 (1)
Br(4)–Cu(2)–Br(6)	100.0 (1)	Br(1a)–Cu(6)–Br(2a)	96.6 (1)
Br(5)–Cu(2)–Br(6)	95.6 (1)	Br(12)–Cu(6)–Br(2a)	100.5 (1)
Br(5)–Cu(3)–Br(6)	91.4 (1)	Cu(1)–Br(1)–Cu(6a)	84.6 (1)
Br(5)–Cu(3)–Br(7)	114.0 (1)	Cu(1)–Br(2)–Cu(6a)	85.2 (1)
Br(6)–Cu(3)–Br(7)	122.7 (1)	Cu(1)–Br(3)–Cu(2)	85.8 (1)
Br(5)–Cu(3)–Br(8)	125.4 (1)	Cu(1)–Br(4)–Cu(2)	85.7 (1)
Br(6)–Cu(3)–Br(8)	112.1 (1)	Cu(2)–Br(5)–Cu(3)	85.9 (1)
Br(7)–Cu(3)–Br(8)	94.2 (1)	Cu(2)–Br(6)–Cu(3)	86.7 (1)
Br(7)–Cu(4)–Br(8)	97.5 (1)	Cu(3)–Br(7)–Cu(4)	84.3 (1)
Br(7)–Cu(4)–Br(9)	133.0 (1)	Cu(3)–Br(8)–Cu(4)	84.0 (1)
Br(8)–Cu(4)–Br(9)	100.8 (1)	Cu(4)–Br(10)–Cu(5)	83.8 (1)
Br(7)–Cu(4)–Br(10)	100.3 (1)	Cu(5)–Br(11)–Cu(6)	85.0 (1)
Br(8)–Cu(4)–Br(10)	133.0 (1)	Cu(5)–Br(12)–Cu(6)	86.1 (1)
Br(9)–Cu(4)–Br(10)	98.0 (1)	Cu(4)–Br(9)–Cu(5)	84.1 (1)
Br(9)–Cu(5)–Br(10)	93.9 (1)		

[a] Symmetry operations: (a) $^1/_2 - x, ^1/_2 - y, z$; (b) $^1/_2 + x, ^1/_2 + y, z$; (c) $^1/_2 + y, -x, ^1/_2 - z$; (d) y, x, z. [b] Symmetry operations: (a) $x, 1 + y, z$.

described by the twist angle, θ, which is defined as the deviation from 90° of the angle between the two $CuBr_2$ planes bisected by the chain axis. This θ measures the angular distortion from tetrahedral of the Cu coordination sphere. The twist angle is 0° at all copper(I) sites, while the twist angle at the two copper(II) sites in the repeat unit are the negative of each other (35.5° for TEM, 36.2° for DEM). The cations in these two structures sit on sites of C_{2v} symmetry and are thus severely disordered. The DEM cation may have C_{2v} symmetry, but the large thermal parameters (Table II) of the C atoms in this cation allude to the presence of disorder. In particular, the ethyl arms of the cation appear to be disordered over two positions, but attempts to model this have failed. In contrast, the TEM cation cannot have C_{2v} symmetry. This results in a more severe disorder problem than in the DEM case; not only the ethyl arms are disordered but also an additional orientational disorder must be taken into account in order to satisfy the site symmetry of the TEM cation. These effects are evident in the large C atom thermal parameters observed in the TEM cation (Table II). The atomic positions and

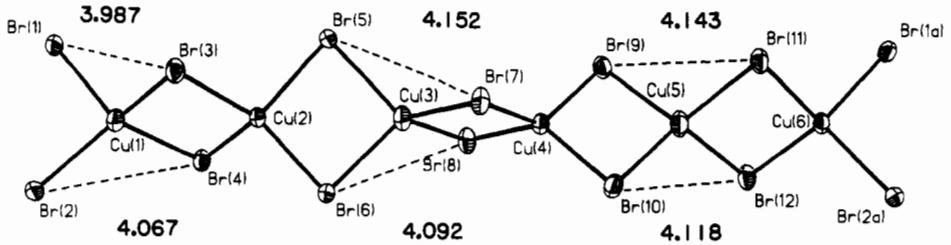

Figure 2. Portion of the $[Cu_2Br_4]_\infty$ chain in $(TEA)Cu_2Br_4$ showing thermal ellipsoids. The Cu(I) sites are labeled Cu(1), Cu(3), and Cu(5) while Cu(2), Cu(4), and Cu(6) are Cu(II). The dashed lines show short Br···Br contacts across the Cu(I) sites.

isotropic thermal parameters are listed in Table II. The bond distances and angles are listed in Table III.

$(TEA)Cu_2Br_4$ belongs to the orthorhombic crystal class and contains lower symmetry chains, in contrast to the chloride analogue and to the previous two bromide salts. An initial room-temperature X-ray data set was collected and a structure solution initiated. The basic chain structure of edge-shared tetrahedra was confirmed. However, disorder of the bromine atoms was evident. For this reason, the low-temperature data set was collected. The resulting refinement revealed chains of $Cu^{II}Br_4^{2-}$ and $Cu^{I}Br_4^{3-}$ anions sharing edges (Figure 2) which run parallel to the *b* axis. There are three copper(I) ions and three copper(II) ions in the repeat unit, with an average Cu(I)–Cu(II) bond distance of 3.290 Å. The coordination geometry around the copper(II) ions is approximately D_{2d}, with the pseudo-S_4 axis of the $Cu^{II}Br_4^{2-}$ species perpendicular to the chain axis. There are three inequivalent copper(II) ions in the repeat unit, each with a different orientation of the pseudo-S_4 axis about the chain axis. The coordination geometry of the three inequivalent copper(I) ions is nearly D_2 but with different extents of flattening of the $CuBr_4^{2-}$ tetrahedra (average trans Br–Cu–Br angles of 133.0, 135.0, and 136.2°, respectively). This will have important consequences in the NIR spectrum of this material (vide infra). The θ values for Cu(2), Cu(4), and Cu(6) are −29.6, −26.1, and −28.3°, respectively. The θ values at the copper(I) sites (not 0° as in the TEM and DEM salts) are −14.3, −9.2, and 8.3° for Cu(1), Cu(3), and Cu(5), respectively. This variety of coordination geometries observed in these chains attests to the softness of the Cu coordination sphere. There is also a great deal of evidence for this in the literature.[15] This softness plays an important role in the chain structure, and the subtle interplay between electronic and cation effects on the chain structure will be discussed below. For later discussion of the magnetic behavior, it is useful to examine short Br···Br contacts between neighboring $Cu^{II}Br_4^{2-}$ tetrahedra *along* the chain. The shortest Br···Br contacts are shown as dashed lines in Figure 2, and the distances range from 3.987 to 4.152 Å. The tetraethylammonium cations are ordered in this structure at low temperature, and there are three TEA cations in the repeat unit. The ethyl arms of each of these cations are fully extended. The first two cations have their pseudo-S_4 axis parallel to the chain axis, while the third cation has its S_4 axis perpendicular to the chain axis. The atomic positions and isotropic thermal parameters are listed in Table II. The bond angles and distances are listed in Table III.

The $(TEA)Cu_2Cl_4$ structure has been previously reported and is analogous to the $(TEM)Cu_2Br_4$ and $(DEM)Cu_2Br_4$ structures reported above. The crystal class is also tetragonal, but the space group is $P4/ncc$. The $[Cu^{II}Cu^{I}Cl_4]_\infty$ chain is very similar to the $(TEM)Cu_2Br_4$ and $(DEM)Cu_2Br_4$ analogues, the only difference being a smaller twist distortion ($\theta = 27.3°$). The copper(II) and copper(I) ions are on sites of D_2 (nearly D_{2d}) and S_4 symmetry, respectively. The Cu(II)–Cu(I) distance is 3.10 Å. The tetraethylammonium cations are sitting on sites of C_4 symmetry and are thus disordered over two orientations. The ethyl arms of the TEA cations are fully extended.

EHMO Band Calculations. The results of the band calculations[11] performed on the $(TEA)Cu_2Cl_4$ salt are shown in Figure 3. For such a chain the basic symmetry elements are a 2-fold

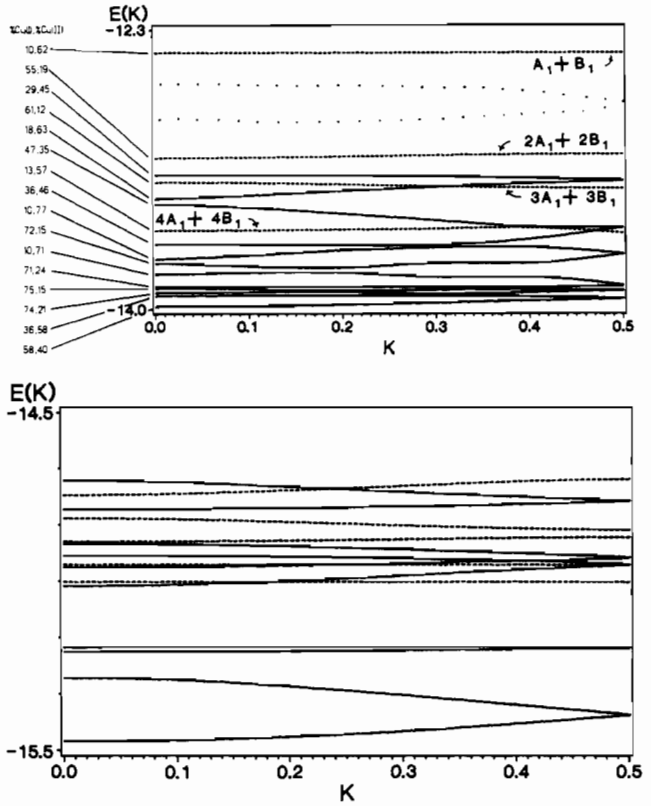

Figure 3. Band structure of $(TEA)Cu_2Cl_4$ for (a, top) the d-block and (b, bottom) the p-block orbitals. Solid lines are bands of A_0 or B_0 symmetry while the dashed lines represent bands with A_1 and B_1 symmetry. The dotted line corresponds to the highest d band for the undistorted structures.

axis along the chain axis, mirror planes perpendicular to the chain axis, and two glide planes along the chain axis. The d-block bands (Figure 3a) consist primarily of copper 3d orbitals with only small contributions from the bridging ligands. These orbitals are antibonding in character. There is also a halide block of crystal orbitals (Figure 3b), consisting of primarily p orbitals on the bridging halides. These orbitals are bonding and/or nonbonding in nature. On the left-hand side of Figure 3a are the compositions of the solid and dashed d-block orbitals at $k = 0$, with respect to the copper(I) and copper(II) contributions. The highest band is degenerate and is primarily copper(II) in character. It is composed of almost exclusively d_{xz} and d_{xy} orbitals on the copper(II) centers. The remaining orbitals in the d-block are centered, to varying degrees, on the copper(I) and copper(II) centers. The orbitals at the top of the ligand block are primarily nonbonding in nature, having large coefficients on the bridging halides only.

The symmetry labels in Figure 3 correspond to the irreducible representations of the point groups D_{2d} ($k = 0, {}^1/_2$) and C_{2v} ($0 < k < {}^1/_2$). The bands depicted by dashed lines correspond to bands of A_1 and B_1 symmetry. The bands depicted by solid lines are of either A_0 or B_0 symmetry. Strictly speaking, the crystal orbitals should transform as the irreducible representations of the space group of the $(TEA)Cu_2Cl_4$ chain. It is fortunate, however, that there is an isomorphic relationship between this space group and the above point groups. This allows the use of the irreducible

(15) Willett, R. D. *Coord. Chem. Rev.* **1991**, *109*, 181.

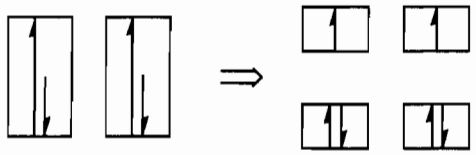

Figure 4. Block diagram showing the electron occupancy of the frontier bands (Figure 3a). The boxes on the extreme left represent the filling of the dotted, parent structure bands. The boxes on the right represent the filling of the top two dashed bands. Each box represents a component of a doubly degenerate band.

representations of the above point groups to describe the symmetry of the crystal orbitals throughout the Brilluoin zone (BZ).

A few important points should be made about the topology of the bands at this point. First of all, the bands depicted by dashed lines belong to doubly degenerate irreducible representations only at the edges of the BZ ($k = 0, {}^1/_2$). On the interior of the BZ these pairs of bands belong to two nondegenerate representations; the degeneracy is an artifact of time reversal symmetry. In C_{2v} ($0 < k < {}^1/_2$), only A_1 and B_1 are susceptible to time reversal symmetry considerations, and so all degenerate bands on the interior of the BZ were assigned as A_1 and B_1. In C_{2v}, bands of A_0 and B_0 symmetry are not susceptible to time reversal symmetry considerations, and thus all nondegenerate bands on the interior of the BZ were assigned to A_0 or B_0 (in terms of the selection rules outlined below, the assignment of these bands as either A_0 or B_0 is inconsequential, and thus no effort was made to do so). All bands at $k = {}^1/_2$ are degenerate due to the glide plane symmetry elements present in the $(TEA)Cu_2Cl_4$ chain (see structure results above).

The selection rules were derived using common group theoretical procedures, and only the results will be summarized here.[16] Transitions $A_1 \rightarrow B_1$ ($B_1 \rightarrow A_1$) are not allowed. The only transitions polarized along the chain axis are of the type $A_1 \rightarrow A_1$ and $B_1 \rightarrow B_1$ and thus include only those transitions from dashed bands to dashed bands. The transitions polarized perpendicular to the chain axis are of the type $A_0 \rightarrow A_1$, $B_0 \rightarrow A_1$, $A_0 \rightarrow B_1$, and $B_0 \rightarrow B_1$. These transitions correspond to all transitions from solid bands to dashed bands. The specific assignment of the A_0 and B_0 bands is thus not important. In summary, dashed $\rightarrow$ dashed transitions are polarized parallel to the chain axis, and solid $\rightarrow$ dashed transitions are polarized perpendicular to the chain axis. These selection rules were worked out on the interior of the BZ, but the same results hold at the zone edges. It should be emphasized that these selection rules are based on the symmetry of the electronic states and do not include the enhancements due to vibrational components of the wave functions.

One of the primary features of the band structure is the band-filling scheme. With 2 copper(I) and 2 copper(II) ions in the unit cell there are 38 d orbital valence electrons with 20 crystal orbitals to place these electrons in. The first 36 electrons fill the lower 18 d-block bands, leaving 2 electrons to place in the top two degenerate bands. In order to predict this band filling, the origin of the chain distortion must be considered. The band structure shown in Figure 3 was calculated for a twist distortion of 27.3° at the copper(II) sites and 0° at the copper(I) sites. The band structure would look quite different if there was a 0° distortion at every copper site, and it is from this geometry that the observed chain geometry is derived. The most important difference, and the only difference that will be considered, concerns the top two dashed bands. In the parent chain geometry, with $\theta = 0°$ at every copper site, these four bands will be degenerate at $k = {}^1/_2$. The top two bands will remain degenerate everywhere else in the BZ, as will the lower two bands. The dotted bands in Figure 3 show the approximate band structure of these four bands in the parent chain structure. The filling of these dotted bands, as well as the structural distortions resulting from these fillings, needs to be considered. Using arguments developed by Whangbo, there are two likely band-filling schemes. The pertinent band-filling scheme

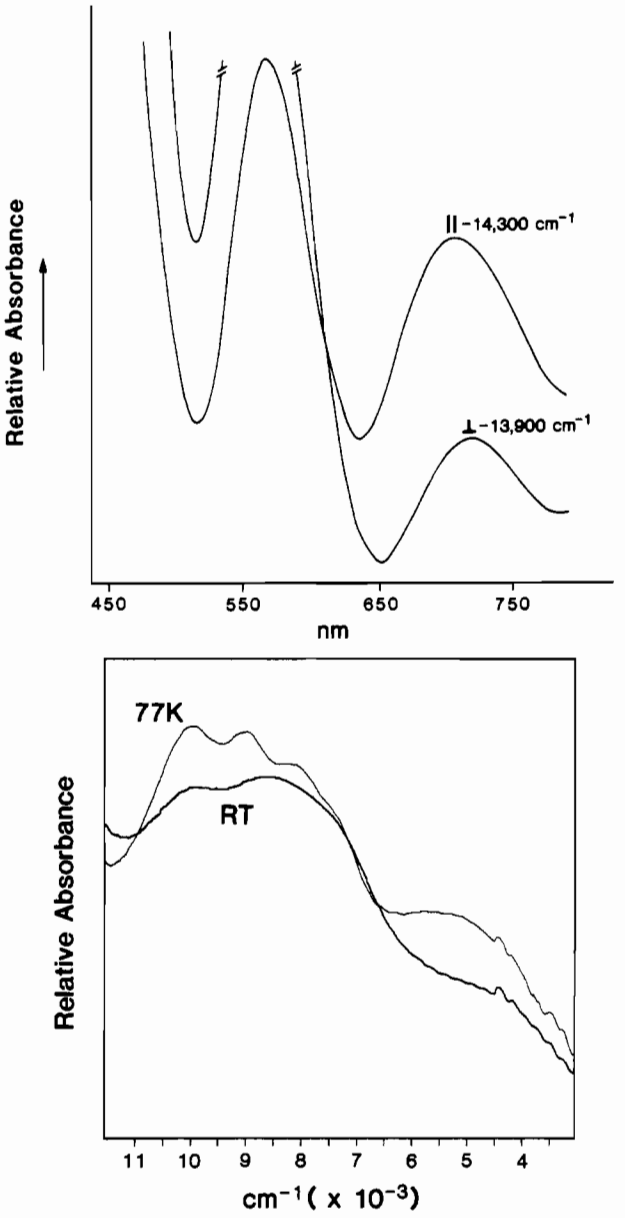

Figure 5. (a, Top) polarized absorption spectrum of $(TEA)Cu_2Br_4$ in the region 450–800 nm. (b, Bottom) room-temperature and 77 K spectra of a melt of $(TEA)Cu_2Br_4$ in the region 3000–12000 cm^{-1}.

is shown in Figure 4. The minimization of electron–electron repulsion is important in these narrow band systems, and this scheme minimizes electron–electron repulsion and represents a high-spin configuration. Such a band filling leads to a $4k_f$ distortion and dimerization of the chain. This distortion is observed in all of the compounds in this paper. (In $(TEA)Cu_2Br_4$ there is an additional distortion leading to three copper(II) sites in the repeat unit, each with a different twist distortion, θ. There are also slight twist distortions about the copper(I) sites. These additional distortions are driven by the cation packing forces, and not additional electronic effects in the anionic chains.) The dimerization is not manifested as the classical pairing of metal atoms but rather as a twisting of the coordination spheres about the copper(II) centers. This twist distortion serves to pair the halide ions within the chain, as well as to localize the positive charge on the copper(II) centers. The localization of charge on the copper(II) centers is what defines these systems as being charge density wave in nature. The dimerization observed in Figure 4 results in an overall stabilization of 0.13 eV in the $(TEA)Cu_2Cl_4$ chloride case. Finally, the postulated band filling resulting from this distortion (right-hand side of Figure 4) places an unpaired electron in every crystal orbital of the top two degenerate bands in Figure 3a. This is an important result and will be used in the

(16) Cotton, F. A. *Chemical Applications of Group Theory*; Wiley-Interscience: New York, 1971.

Table IV. Summary of Important Structural and Spectral Parameters for the Title Compounds

compd	twist distortion θ, deg	trans angle, deg	ligand field and IVCT transitions, cm^{-1}	charge-transfer transitions, cm^{-1}
$(TEA)Cu_2Cl_4$	27.3	133.9	5800, 10000, 15870	20000,[b] 23800[c]
$(TEA)Cu_2Br_4$	28.0[a]	134.7[a]	5000, 7500, 8100, 9000, 9950, 13900	17400,[d] 20400[b]
$(TEM)Cu_2Br_4$	35.5	140.6	6500, 9200, 15400	20000,[b] 22200[c]
$(DEM)Cu_2Br_4$	36.2	140.2	6400, 10200, 14800	19500,[b] 21000[c]

[a] Average value. [b] Onset of absorption edge. [c] Shoulder. [d] Sharp maxima.

Discussion to rationalize the magnetic behavior.

Absorption Spectroscopy. The absorption spectra for the $(TEA)Cu_2Br_4$ salt are shown in Figure 5. The polarized absorption spectrum, in the visible region of the spectrum, is shown in Figure 5a. Two prominent bands are observed in this spectrum: one broad band is observed at 720 nm (13900 cm^{-1}) and one narrow band at 575 nm (17400 cm^{-1}). The former band shows strong polarization parallel to the chain axis, while the latter band is polarized perpendicular to the chain axis. In addition to these peaks, a very intense absorption edge is observed at approximately 490 nm (20400 cm^{-1}). The room-temperature and 77 K spectra, in the NIR region, are shown in Figure 5b. The 77 K spectrum reveals five peaks at 9950, 9000, 8100, 7500, and 5000 cm^{-1}, while only three peaks at 10000, 8500, and 5000 cm^{-1} are resolved in the room-temperature spectrum.

The absorption spectrum for $(TEA)Cu_2Cl_4$ is shown in Figure 6. The polarized absorption spectrum, in the near-IR region of the spectrum, is shown in Figure 6a. For the perpendicular polarization two broad peaks are observed at 10000 and 5800 cm^{-1}. In the parallel polarization two peaks are also observed at about 10000 and 5800 cm^{-1}, but some additional structure is observed on the peak at 10000 cm^{-1}. Also, the left-hand side of the spectrum shows the tail of a higher energy absorption in the parallel polarization. The room-temperature visible spectrum of the melt is shown in Figure 6b. A broad absorption is observed at 630 nm (15870 cm^{-1}). The onset of an intense absorption edge is observed at approximately 20000 cm^{-1}, with a shoulder near 23800 cm^{-1}.

The absorption spectra of the melts of $(DEM)Cu_2Br_4$ and $(TEM)Cu_2Br_4$ are similar in appearance to that of the $(TEA)Cu_2Cl_4$ salt, and their values are summarized, along with all the above spectroscopic values, in Table IV.

Before making detailed assignments, it is instructive to compare these results with those obtained for isolated Cu(I) and Cu(II) species. The ligand field absorption spectrum of a D_{2d}, CuX_4^{2-} chromophore typically shows two broad bands, the higher energy band assigned to the $^2B_2 \rightarrow {}^2A_1$ ($d_{z^2} \rightarrow d_{x^2-y^2}$) and $^2B_2 \rightarrow {}^2B_1$ ($d_{xy} \rightarrow d_{x^2-y^2}$) transitions and the lower energy band assigned to the $^2B_2 \rightarrow {}^2E$ ($d_{xz},d_{yz} \rightarrow d_{x^2-y^2}$) transition. The energy of these transitions has been shown to be directly proportional to the CuX_4^{2-} trans angle. For chloro complexes with trans angles from 125 to 140°, the two bands occur in the range 9000–11000 and 6000–9000 cm^{-1}, respectively.[17] In contrast, there is no ligand field spectrum for the d^{10} CuX_4^{3-} chromophore.

The charge-transfer spectrum of the D_{2d} $CuBr_4^{2-}$ chromophore[18] generally shows a strong absorption in the visible region of the spectrum, consisting of two dominant bands. These bands occur at approximately 17000 and 19000 cm^{-1} and correspond to π(nonbonding) $\rightarrow d_{x^2-y^2}$ and π(bonding) $\rightarrow d_{x^2-y^2}$ ligand to metal charge-transfer transitions. In the chloride analogues[19] these transitions occur at approximately 25000 and 32000 cm^{-1}. The CuX_4^{3-} chromophore has no such charge-transfer states. Instead, it exhibits metal to ligand charge transfer in the UV region of the spectrum.

Spectral Assignments. A very simple picture of the energy level diagram resulting when the CuX_4^{2-} and CuX_4^{3-} chromophores form a $Cu^{II}Cu^{I}X_6^{3-}$ dimer is shown in Figure 7. A first approximation of the ligand field absorption spectrum based on this diagram shows that the original CuX_4^{2-} ligand field spectrum is still present (left-hand side of Figure 7). In addition, new intervalence charge-transfer bands will be present and are indicated by the IVCT arrow. This simple picture will be altered by perturbation of the copper(II) d orbitals caused by the mixing in of the copper(I) d orbitals and vice versa. The results of the EHMO calculations, described below, will be used to ascertain the effect of this mixing.

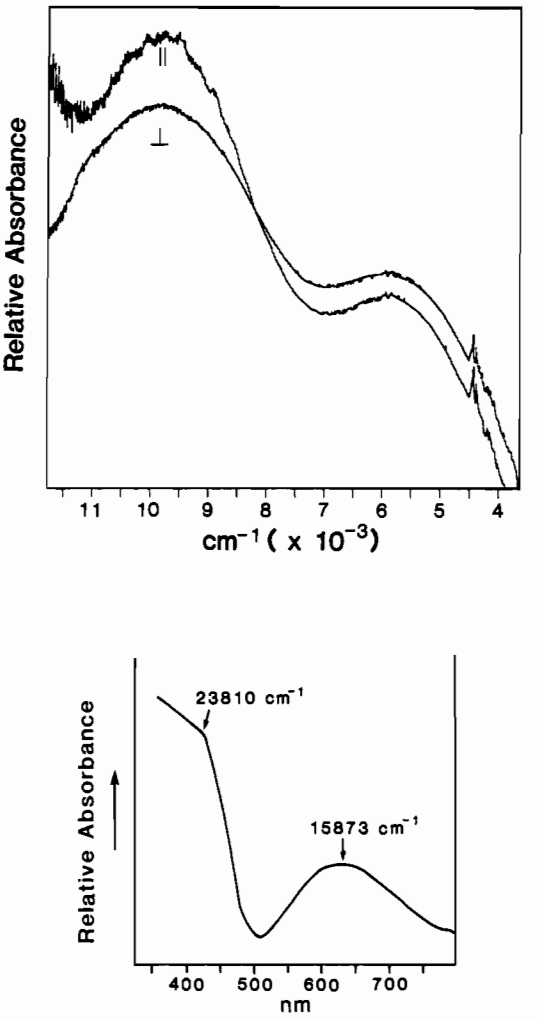

Figure 6. (a, Top) room-temperature polarized absorption spectrum of $(TEA)Cu_2Cl_4$ in the region 3000–12000 cm^{-1}. (b, Bottom) room-temperature spectrum of a melt of $(TEA)Cu_2Cl_4$ in the region 350–800 nm.

The assignment of the absorption spectra will be made in terms of the band picture presented in Figure 3. Two classes of transitions are expected: transitions within the d-block to the highest unoccupied band orbital (HUBO) and transitions from within the p-block to the HUBO. All of the compounds exhibit several transitions in the NIR region, as well as a single broad transition at the NIR–visible border. The only other notable feature in the absorption spectrum, except for in $(TEA)Cu_2Br_4$, is the absorption edge occurring at the visible–UV border. The $(TEA)Cu_2Br_4$ salt shows a sharp maxima at about 17000 cm^{-1}. The transitions in the NIR region may be thought of as two broad peaks, with varying degrees of structure. For all compounds, Cl and Br analogues as well, the approximate position of these envelopes is

(17) Harlow, R. L.; Wells, W. J., III; Hitchman, M. A. *Inorg. Chem.* **1988**, *27*, 894.
(18) Scott, B.; Willett, R. D. *J. Am. Chem. Soc.* **1991**, *113*, 5253.
(19) Smith, D. W. *Coord. Chem. Rev.* **1976**, *21*, 93.

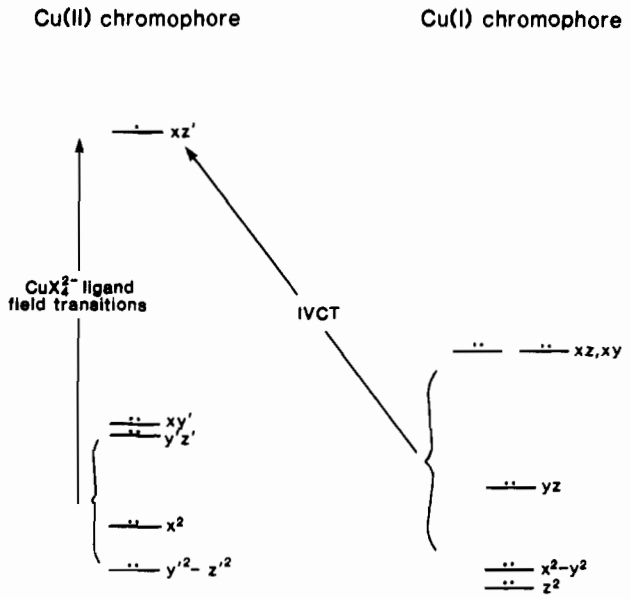

Figure 7. Energy level diagram of the CuX_4^{2-} and CuX_4^{3-} chromophores showing ligand field transitions. The S_4 CuX_4^{3-} species has the following coordinate system: the x axis (chain axis) is coincident with the S_4 axis, and the xz and yz planes are coincident with the two Cu^IX_2 planes bisected by the S_4 axis. The D_2 CuX_4^{2-} species has the following coordinate system: the x axis is coincident with the C_2 axis lying along the chain axis, with the y' and z' axes corresponding to the two C_2 axes perpendicular to the chain axis. When $\theta = 0°$, the y' and z' axes are equivalent to the y and z axes of the CuX_4^{3-} species (vide supra).

constant. Likewise, the position of the broad absorption at the visible–NIR border is approximately the same for all analogues. The ligand field strengths of the Cl and Br ions are nearly the same, and thus the energies of the ligand field transitions should be approximately the same. The two transitions in the NIR region and the transition at the near-IR–visible border will be assigned to transitions arising from orbitals in the d-block to the HUBO. Strictly speaking, these ligand field transitions are LaPorte rule forbidden and occur only through vibronic coupling and ligand p orbital/d orbital mixing. Assignments made solely on the selection rules outlined above are hazardous; these selection rules will be used along with vibronic coupling and oscillator strength arguments to make the final assignments.

(i) Ligand-to-Metal Charge-Transfer Transitions. The sharp maxima at 17 000 cm^{-1} in the $(TEA)Cu_2Br_4$ salt, as well as the absorption edges observed in all analogues, will be assigned to transitions arising from the ligand block to the HUBO. The sharp peak at 17 000 cm^{-1} in $(TEA)Cu_2Br_4$ is quite intense in both the parallel and perpendicular polarizations. It is tentatively assigned as arising from the first set of closely spaced bands at the top of the p-block. The presence of both solid and dashed bands account for the strong intensity of both polarizations. The fact that this transition is not observed at this energy in the other bromide analogues is explained by the large difference in the $CuBr_4^{2-}$ geometry between the TEA and the TEM and DEM analogues; the HUBO is pushed higher in energy in the TEM and DEM analogues due to the higher trans angles in these salts. The larger trans angle serves to provide a more effective antibonding interaction between the bridging halide orbitals and the d_{xz} and d_{xy} orbitals of the HUBO. In addition, the HUBO has a small copper(I) character, and it is possible that the larger trans angle in the DEM and TEM analogues allows a larger Cu(I) contribution and thus greater destabilization of the HUBO. The overall destabilization resulting from these two effects results in higher energy for the p(nonbonding) → HUBO transition in the DEM and TEM analogues, and thus the absorption edge (22 000 cm^{-1}) in these salts is assigned to this transition. In the $(TEA)Cu_2Cl_4$ salt the energy of this transition is expected to be of higher energy, not so much because of the trans angle difference, but rather due to the higher energy charge transfer associated with the chloride ion.

(ii) Localized d–d Transition. The broad transition at 6000 cm^{-1} in the $(TEA)Cu_2Cl_4$ salt is only slightly more intense, and broad, in the perpendicular polarization. Transitions arising from the first two dashed bands and the first two solid bands (below the HUBO) show parallel and perpendicular polarizations, respectively. In addition, these four bands lie close in energy. The band at 6000 cm^{-1} is tentatively assigned to the $2A_1 + 2B_2$, $3A_1 + 3B_1$, and surrounding A_0 and $B_0 \rightarrow A_1 + B_1$ transitions.

The band at 10 000 cm^{-1} in the $(TEA)Cu_2Cl_4$ salt shows stronger intensity, and additional structure, in the parallel polarization. The perpendicular polarization shows little structure. The assignment of the band at 6000 cm^{-1} leaves the $4A_1 + 4B_1$ and surrounding A_0 and $B_0 \rightarrow A_1 + B_1$ transitions for the 10 000 cm^{-1} band assignment. The additional structure in the parallel polarization is explained by the bands of A_0 and B_0 symmetry surrounding the lone $4A_1 + 4B_1$ band. Transitions arising from these solid bands should be polarized perpendicular to the chain axis, but it is postulated that vibronic coupling mechanisms account for a parallel component. The transition at 10 000 cm^{-1} is thus assigned to the $4A_1 + 4B_1 \rightarrow A_1 + B_1$ and surrounding A_0 and $B_0 \rightarrow A_1 + B_1$ transitions.

Although no band calculations have been carried out on the $(TEA)Cu_2Br_4$ analogue, the assignment of its spectrum should be quite similar to that of the chloride analogue. The major differences are the larger trans angle about the copper(II) center and the larger repeat unit in the bromide analogue. The greater number of copper atoms in the repeat unit of the bromide analogue results in a greater number of crystal orbitals in the d-block and thus more structure to these transitions. This is observed in comparing the spectra of $(TEA)Cu_2Cl_4$ (Figure 5b) and $(TEA)Cu_2Br_4$ (Figure 6a). The larger trans angles in the bromide analogue should result in shifting its transitions to lower energies, and the spread of trans angles (133.0–136.2°) leads to the structure observed in the transitions of the $(TEA)Cu_2Br_4$ analogue (Figure 6a). This is observed by comparing the data for the chloride and bromide analogues in Table IV.

(iii) Intervalence Transition. The broad band at 15 780 cm^{-1} in the $(TEA)Cu_2Cl_4$ salt shows a relatively strong polarization in the parallel orientation, as can be observed at the left-hand edge of the spectrum in Figure 6a (the full band is shown in Figure 6b). This band is assigned to $A_0 + B_0 \rightarrow A_1 + B_1$ transitions arising from the tight group of solid bands at the bottom of the d-block. According to the selection rules these transitions are polarized perpendicular to the chain axis. However, vibronic coupling mechanisms almost surely account for a parallel component. It may be argued that the greater intensity in the parallel polarization is explained by the stronger oscillator strength of the transitions polarized along the chain axis. The Cu(I)–Cu(II) distance of 3.1 Å accounts for a large transition dipole moment and thus a large oscillator strength. In the perpendicular polarization, however, the transition is localized to a greater extent on the copper(II) center, thus having a much smaller oscillator strength. The fact that there is still a small amount of intensity remaining in the perpendicular polarization is probably a result of copper(II) character delocalized out onto the bridging halide.

Electrical Conductivities. These measurements yielded room-temperature resistivities of 1.0×10^5 Ω cm for $(TEA)Cu_2Cl_4$ and 3.3×10^6 Ω cm for $(TEA)Cu_2Br_4$.

Magnetic Susceptibilities. A plot of the magnetic susceptibility vs temperature for $(TEA)Cu_2Br_4$ is shown in Figure 8. The solid curve is the calculated susceptibility as a function of temperature, g and J. This curve was calculated using the Pade Heisenberg $s = {}^1/_2$ high-temperature series expansion.[20] This fit to the data yielded $J = -1.8$ K and $g = 2.09$. The source of this antiferromagnetic coupling is attributed to the short Br···Br contacts shown in Figure 2. This conclusion is based on an analogous system of $CuBr_4^{2-}$ monomers which have Br···Br contacts of 4.10 and 4.30 Å. These contacts result in exchange pathways with $J/k = -6.64$ K (4.10 Å) and $J/k = -0.66$ K (4.30 Å).[21]

(20) Baker, G. A., Jr.; Rushbrooke, G. S.; Gilbert, H. E. *Phys. Rev. A* **1964**, *135*, 1272.

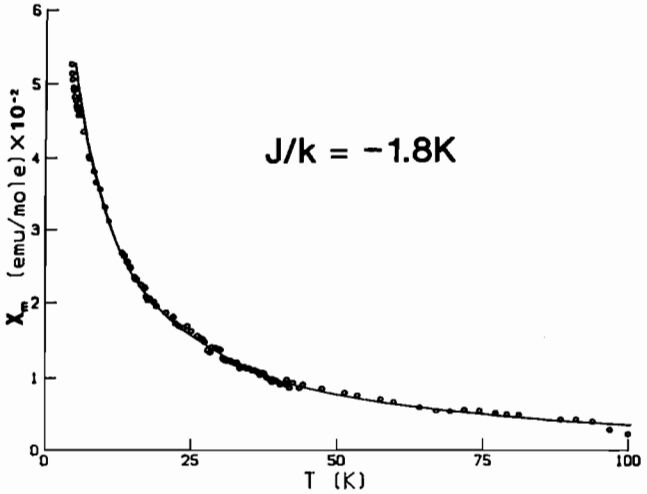

Figure 8. Plot of the magnetic susceptibility versus temperature for $(TEA)Cu_2Br_4$.

Discussion

The absorption spectral data presented in this paper make an excellent case for the presence of intervalence charge transfer in the title compounds. The two broad absorption envelopes in the NIR region and the broad absorption band at the visible–NIR border were assigned to transitions within the d-block. These transitions arise from orbitals with varying degrees of copper(I) and copper(II) characters (Figure 3a) and terminate on the HUBO, which is predominantly copper(II) in character. All of these transitions thus have some intervalence character. The original CuX_4^{2-} ligand field transitions, although perturbed via mixing with the copper(I) d orbitals, are still present within the lower energy absorption envelopes, along with the new intervalence transitions. In addition, a new band, not present in either CuX_4^{n-} chromophore taken separately, is observed at the visible–NIR border.

The experimental evidence strongly supports a Robin and Day class II assignment for the title compounds. The X-ray diffraction results show the Cu(I) and Cu(II) ions to be in ligand fields of nearly identical symmetry, with the Cu(I)–X and Cu(II)–X bond distances showing approximately a 0.1 Å difference. The band calculations point to a small degree of delocalization; these calculations revealed that the HUBO contains a 10% copper(I) character (Figure 3a). The conductivity results showed that the title compounds are semiconducting. As pointed out above, the absorption experiments revealed the presence of intervalence charge-transfer bands along with the slightly perturbed CuX_4^{2-} transitions. All of these results fall right in step with the Robin and Day class II definitions, thus justifying such a classification.

The structural distortions observed in the title compounds have much in common with Wolfframs Red salt and its derivatives (PtX). The latter class of compounds consist of chains of alternating, $Pt^{II}L_4$ and $Pt^{IV}L_4X_2$ units. These chains may be thought of as being derived from a linear chain of $Pt^{III}L_4X_2$ ions which have undergone a pairing of axial halide ions leading to a mixed-valence Pt(II)–Pt(IV) system.[22] These systems are Peierls-distorted charge density wave systems and possess intervalence charge-transfer bands. The title compounds have undergone a similar distortion involving the pairing of halide ions, but it is manifested as a twist about the chain axis as well as a dimerization of the halide ions along the chain. The reason for the difference in the nature of the pairing distortion is 2-fold: (1) the chains in the title compounds are made up of edge-shared tetrahedra whereas the Pt chains are made up of stacked planar complexes bridged with halide ions; (2) the copper coordination sphere is very soft and is subject to a Jahn-Teller distortion from T_d symmetry, resulting in a twist distortion. These two factors explain why a pairing of the halide ions in the title compounds is more efficiently achieved with a twist distortion, and not a simple halide dimerization along the chain. The presence of the IVCT band in the title compounds, as well as the structural results, supports the charge density ground state for the copper halide chains.

Recent work on the PtX materials have demonstrated the presence of photoinduced defects in the chain structures.[23] Such defects are probably present in the title compounds as well. Additional work is planned to search for such behavior.

The shallow depth of the potential well (0.13 eV) resulting from the twist distortion indicates that cation–chain interactions play an important role in determining the structure. The dimerization observed in the mixed-valence chains appears to arise from $4k_f$ distortions brought on by partially filled bands in the $(TEM)Cu_2Br_4$, $(DEM)Cu_2Br_4$, and $(TEA)Cu_2Cl_4$ salts. The additional distortions in the $(TEA)Cu_2Br_4$ compound are dominated by crystal packing forces. In the first three compounds the difference in the cation does not affect the basic chain structure. One possible explanation for this is the severely disordered cations in these structures. It is postulated that the chains in these structures experience a uniform time-averaged force from the disordered cations, and thus any cation effect is washed out. Thus, these two bromide analogues, TEM and DEM, have remarkably similar chain geometries. The fact that $(TEA)Cu_2Cl_4$ has a 9° smaller twist distortion, relative to $(TEM)Cu_2Br_4$ and $(DEM)Cu_2Br_4$, is explained by the bridging halide ion; in the bromide analogues the dispersion of the band structure is greater, and thus the distortion is larger. In $(TEA)Cu_2Br_4$ the chain structure does not agree with any of the distortions predicted by the band calculations. In this structure the cations are ordered. The fact that every third cation is flipped on its side also creates a less symmetrical channel for the copper bromide chain in the TEA analogue. It is postulated that the interactions of these ordered cations with the mixed-valence chain outweigh the electronic effects, resulting in a lower symmetry chain.

The interplay between electronic and cation effects on the structures of one-dimensional chains was recently studied in another system by Corbett et al.[24] This work focused on the compounds with the stoichiometry $LiScI_3$ and $Na_{0.5}ScI_3$. These materials are linear chains of Sc atoms tribridged by iodine, with either Li or Na as a counterion. The Li salt, a d^1 system, is a uniform linear chain. The electronic factors predict that this compound should undergo a pairing distortion, but in fact the ScI_3 chains remains uniform. On the other hand, the $Na_{0.5}ScI_3$ system ($d^{0.5}$) possesses a ScI_3 linear chain that has undergone a Peierls distortion, resulting in Sc–Sc bond alternation along the chain axis. The authors postulate that strong interactions between the Li and I atoms stiffen the lattice and preclude the Peierls distortion. It is important to understand such cation–chain interactions if chain structure and, hence, physical properties are to be controlled. Studies probing such relationships in copper halide mixed-valence chains are currently underway.

If some of the spin present on the copper(II) center were delocalized onto the copper(I) center, as suggested by the band calculations, an exchange pathway similar to that encountered in $Cu_2X_6^{2-}$ dimers could be expected. The geometry of the bridges in the title compounds is similar to a series of twisted dimers, which show ferromagnetic coupling.[25] The susceptibility data, however, show a weak antiferromagnetic coupling ($J/k = -1.8$ K for $(TEA)Cu_2Br_4$). This points to the dominant exchange pathway being through the short Br···Br contacts along the chain axis (vide supra). Therefore, the magnetic exchange is best thought of in terms of orbitals localized on the Cu(II) centers and not in terms of a band picture.

(21) Patyal, B. R.; Scott, B. L.; Willett, R. D. *Phys. Rev. B* **1990**, *41*, 1657.
(22) Whangbo, M.-H. *Acc. Chem. Res.* **1983**, *16*, 95.
(23) Donohoe, R. J.; Tait, C. D.; Swanson, B. I. *Chem. Mater.* **1990**, *2*, 315 and references therein.
(24) (a) Corbett, J. D.; Dorhout, P. K.; Dudis, D. S.; Lachgar, A. *Inorg. Chem.* **1991**, *30*, 3321. (b) Dorhout, P. K.; Corbett, J. D. *Inorg. Chem.* **1991**, *30*, 3326.
(25) Willett, R. D.; Grigereit, T.; Halvorson, K.; Scott, B. *Proc.—Indian Acad. Sci., Chem. Sci.* **1987**, *98*, 147.

Conclusions

The title compounds are Peierls distorted, pinned charge density wave systems with $4k_f$ superstructures. The mixed-valence chain structures were found to be dominated by electronic effects when disordered cations were present ($4k_f$ systems) but by crystal packing forces producing an additional distortion when ordered cations were present ($(TEA)Cu_2Br_4$). The presence of a strong intervalence charge-transfer band in the low-energy end of the visible region was demonstrated through absorption spectral data and EHMO band calculations. A picture utilizing localized magnetic orbitals offers the best description of the magnetic exchange. All of the experimental evidence presented in this work strongly indicate that the title compounds belong to Robin and Day class II.

Acknowledgment. This research was supported by NSF Grant DMR-8803382 and by the donors of the Petroleum Research Fund, administered by the American Chemical Society. The X-ray diffraction facility was established through funds provided by NSF Grant CHE-8408407 and The Boeing Co. Work at Argonne National Laboratory is supported by the Office of Basic Energy Sciences, Division of Materials Sciences, U.S. Department of Energy, under Contract W-31-109-ENG-38. We thank Professor Roald Hoffmann for making details of the EHMO calculation on $(TEA)Cu_2Cl_4$ available to us. We also thank Mr. Ping Zhou for collecting the magnetic susceptibility data.

Registry No. $(TEM)Cu_2Br_4$, 141170-87-8; $(TEA)Cu_2Br_4$, 141170-88-9; $(DEM)Cu_2Br_4$, 141170-89-0; $(TEA)Cu_2Cl_4$, 110488-61-4.

Supplementary Material Available: Tables of X-ray data collection parameters, bond lengths and angles for the cations, anisotropic thermal parameters for non-hydrogen atoms, and hydrogen atom positions and isotropic thermal parameters for all three structures (11 pages); structure factor tables for all three structures (26 pages). Ordering information is given on any current masthead page.

Contribution from the Department of Chemistry, University of California, Irvine, California 92717

Formation of Bimetallic, Trimetallic, and Pentametallic Yttrium Methoxide and Methoxide Oxide Complexes from Reactions of Alkali-Metal Methoxides with Bis(cyclopentadienyl)yttrium Chloride

William J. Evans,* Mark S. Sollberger, Julie L. Shreeve, Jeffrey M. Olofson, John H. Hain, Jr., and Joseph W. Ziller

Received November 14, 1991

The superficially simple metathetical reaction of $(C_5H_5)_2YCl(THF)$ with alkali-metal methoxides has been found to form a variety of products and product mixtures depending on reaction conditions. $(C_5H_5)_2YCl(THF)$ reacts with NaOMe to form $[(C_5H_5)_2Y(\mu\text{-OMe})]_2$ (**1**) in 80–95% yield depending on the method of isolation of the product. **1** can be generated analogously from KOMe in up to 75% yield depending on reaction conditions and the source of KOMe. The primary byproduct in KOMe reactions, which can be isolated in up to 20% yield, was identified as the trimetallic anion $\{[(C_5H_5)_2Y(\mu\text{-OMe})]_2[(C_5H_5)_2Y](\mu_3\text{-O})\}^-$ (**2**). The yield of **2** can be increased to as high as 70% by varying the reaction conditions and the $(C_5H_5)_2YCl(THF)$ to KOMe stoichiometry. Me_2O has been isolated as a byproduct in this oxide-forming reaction. The previously characterized pentametallic complex $(C_5H_5)_5Y_5(\mu\text{-OMe})_4(\mu_3\text{-OMe})_4(\mu_5\text{-O})$ (**3**) is also formed in this reaction system. **3** can be obtained in high yield from the reaction of $(C_5H_5)YCl_2(THF)_3$, generated in situ, with 2 equiv of *Na*OMe in THF at reflux or from the reaction of $(C_5H_5)_2YCl(THF)$ and MeOH-solvated KOMe. Other cyclopentadienyl alkoxide products are also formed in these reactions, and the product mixtures are highly dependent upon the particular alkali-metal alkoxide used, its method of preparation, the reaction time and temperature, reagent concentrations, and workup procedure. The direct formation of the polymetallic products from **1** and methoxide reagents has been investigated and further shows the complexity of this system. Crystallographic data have been obtained on **1–3** as well as the (trimethylsilyl)cyclopentadienyl analogue of **1** $[(C_5H_4SiMe_3)_2Y(\mu\text{-OMe})]_2$ (**4**) and its chloride precursor $[(C_5H_4SiMe_3)_2Y(\mu\text{-Cl})]_2$ (**5**). Complexes **1**, **4**, and **5** are comprised of $(C_5H_4R)_2Y$ (R = H, $SiMe_3$) bent metallocene units bridged by methoxide or chloride ligands. In **2**, three $(C_5H_5)_2Y$ bent metallocene units define a triangle with two sides bridged by methoxide groups. Near the third side in the interior of the triangle and coplanar with the yttrium atoms is a μ_3-oxide ligand. **2** crystallized with the countercation $\{[(THF)_3Na]_2(\mu\text{-}C_5H_5)\}$ in which a bridging C_5H_5 group is sandwiched between two $Na(THF)_3$ moieties. $[(C_5H_5)_2Y(\mu\text{-OMe})]_2$ crystallized from toluene in space group $P\bar{1}$ with unit cell dimensions a = 16.747 (11) Å, b = 27.351 (14) Å, c = 8.404 (4) Å, α = 90.00 (4)°, β = 109.49 (4)°, γ = 90.05 (5)°, V = 3629 (3) Å^3, and Z = 6 for D_{calcd} = 1.14 g cm^{-3}. $\{[(C_5H_5)_2Y)]_3(OMe)_2O\}\{[(THF)_3Na]_2(C_5H_5)\}$ crystallized from THF in space group *Pnam* with unit cell dimensions a = 18.854 (6) Å, b = 15.803 (3) Å, c = 22.355 (8) Å, and Z = 4 for D_{calcd} = 1.28 g cm^{-3}. $[(C_5H_4SiMe_3)_2Y(\mu\text{-OMe})]_2$ crystallized from benzene with two molecules of benzene in the lattice in space group $C2/c$ with unit cell dimensions a = 24.930 (3) Å, b = 13.735 (2) Å, c = 14.764 (2) Å, β = 91.90 (1)°, V = 5052 (1) Å^3, and Z = 4 for D_{calcd} = 1.24 g cm^{-3}. Least-squares refinement based on 3653 observed reflections led to a final R_F value of 5.3%. $[(C_5H_4SiMe_3)_2Y(\mu\text{-Cl})]_2$ crystallized from benzene in space group $P\bar{1}$ with a = 8.676 (2) Å, b = 9.763 (2) Å, c = 12.487 (2) Å, α = 70.38 (1)°, β = 76.69 (1)°, γ = 88.67 (1)°, V = 967.7 (3) Å^3, and Z = 1 for D_{calcd} = 1.37 g cm^{-3}. Least-squares refinement of the model based on 3285 reflections converged to a final R_F = 4.3%.

Introduction

Recently, we have been studying the synthesis of oxygen-stabilized organoyttrium and organolanthanide complexes[1-8] in order to obtain more robust compounds with which to exploit the unusual chemistry of these metals.[9-12] In particular, we have been ex-

(1) Evans, W. J.; Sollberger, M. S. *J. Am. Chem. Soc.* **1986**, *108*, 6095–6096.
(2) Evans, W. J.; Sollberger, M. S.; Hanusa, T. P. *J. Am. Chem. Soc.* **1988**, *110*, 1841–1850.
(3) Evans, W. J.; Sollberger, M. S. *Inorg. Chem.* **1988**, *27*, 4417–4423.
(4) Evans, W. J.; Deming, T. J.; Olofson, J. M.; Ziller, J. W. *Inorg. Chem.* **1989**, *28*, 4027–4034.
(5) Evans, W. J.; Olofson, J. M.; Ziller, J. W. *Inorg. Chem.* **1989**, *28*, 4308–4309.
(6) Gradeff, P. S.; Yunlu, K.; Deming, T. J.; Olofson, J. M.; Doedens, R. J.; Evans, W. J. *Inorg. Chem.* **1990**, *29*, 420–424.
(7) Evans, W. J.; Olofson, J. M.; Ziller, J. W. *J. Am. Chem. Soc.* **1990**, *112*, 2308–2314.
(8) Evans, W. J.; Golden, R. E.; Ziller, J. W. *Inorg. Chem.* **1991**, *30*, 4963–4968.
(9) Evans, W. J. *Adv. Organomet. Chem.* **1985**, *24*, 131–177.
(10) Evans, W. J. *Polyhedron* **1987**, *6*, 803–835.
(11) Marks, T. J.; Ernst, R. D. In *Comprehensive Organometallic Chemistry*; Wilkinson, G., Stone, F. G. A., Abel, E. W., Eds.; Pergamon Press: New York, 1982; Chapter 21.

0020-1669/92/1331-2492$03.00/0